JGR Atmospheres

RESEARCH ARTICLE
10.1029/2022JD038246

Ambient Conditions of Winter Thunderstorms in Japan to Reproduce Observed Gamma-Ray Glow Energy Spectra

G. S. Diniz[1], Y. Wada[2], Y. Ohira[3], K. Nakazawa[4], M. Tsurumi[5,6], and T. Enoto[1,6]

[1]Department of Physics, Graduate School of Science, Kyoto University, Kyoto, Japan, [2]Division of Electrical, Electronic and Infocommunications Engineering Graduate School of Engineering, Osaka University, Osaka, Japan, [3]Department of Earth and Planetary Environmental Science, The University of Tokyo, Tokyo, Japan, [4]Kobayashi-Maskawa Institute for the Origin of Particles and the Universe, Nagoya University, Nagoya, Japan, [5]Graduate School of Science and Engineering, Aoyama Gakuin University, Sagamihara, Japan, [6]Extreme Natural Phenomena RIKEN Hakubi Research Team, RIKEN Cluster for Pioneering Research, Saitama, Japan

Key Points:

- We use Monte Carlo simulations of electron and gamma-ray interactions in thunderstorms to explain observed gamma-ray glows
- We successfully simulated gamma-ray glow spectra and extracted an acceptable set of ambient atmospheric factors of the glow
- Fit configurations have electric fields as ~0.30 MV/m with a ~1 km size scale and a null field region of ~0.5 km below that

Correspondence to:
G. S. Diniz,
diniz.gabriel.58j@st.kyoto-u.ac.jp

Citation:
Diniz, G. S., Wada, Y., Ohira, Y., Nakazawa, K., Tsurumi, M., & Enoto, T. (2023). Ambient conditions of winter thunderstorms in Japan to reproduce observed gamma-ray glow energy spectra. *Journal of Geophysical Research: Atmospheres*, *128*, e2022JD038246. https://doi.org/10.1029/2022JD038246

Received 23 NOV 2022
Accepted 24 APR 2023

Abstract Electric field of thunderclouds modifies components and energy spectra of the cosmic-ray air shower. In particular, thunderstorms accelerate charged particles, resulting in an enhancement of gamma-ray fluxes on the ground, known as a gamma-ray glow. This phenomenon has been observed in recent years by the Gamma-Ray Observation of Winter THunderclouds collaboration from winter thunderstorms in the Hokuriku area of Japan. The present work examines the ambient conditions required to produce spectral features of the previously detected gamma-ray glows, by using Monte Carlo simulations of particle interactions in the atmosphere. We focus on three parameters, the strength and length of the electric field, and the length of a null-field attenuation region below the electrified region. The average spectrum of observed gamma-ray glows in winter thunderstorms of Japan requires an electric field intensity close to 0.31 MV/m, slightly exceeding the Relativistic Runaway Electron Avalanche threshold of 0.284 MV/m. The vertical size of the electric field region should be comparable to 1 km. The estimated attenuation region size is 300–500 m, necessary to reduce the low-energy photon flux of the average gamma-ray glows. There is still a wide range of acceptable parameter sets with degeneracy to make a similar spectrum.

Plain Language Summary Thunderclouds modify the incident cosmic-ray flux due to their electric field. In particular, thunderstorms accelerate charged particles inducing enhancement of the gamma-ray flux at the ground, known as the gamma-ray glow. Throughout recent years, the community observes gamma-ray glows on the Japanese Hokuriku coast. This paper examines the ambient conditions required to produce the characteristic gamma-ray glow spectrum using Monte Carlo simulation. We focus on the electric field strength, and electric field length and introduced a null-field attenuation region following previously reported features of Japanese winter thunderclouds. We conclude that most observed gamma-ray glows at the Hokuriku region require electric fields close to 0.32 MV/m along approximately 1 km and an attenuation region of 300–500 m to reproduce the observations. Finally, the three studied variables can be differently combined to generate similar spectra regarding a space of phase of three coordinates being electric field strength, electric field length, and attenuation space length.

1. Introduction

Thunderclouds and lightning are thought to become a local energy source through intense electric fields to charged particles in the atmosphere, for example, cosmic-rays extensive air showers. Accelerated electrons result in gamma-ray flux enhancements recorded at the ground, and airborne experiments (Chilingarian, 2013; Chilingarian et al., 2017; Kelley et al., 2015; Kochkin et al., 2017; Østgaard et al., 2019; Torii et al., 2002; Tsuchiya et al., 2007, 2012; Wada et al., 2018). Such gamma-ray enhancement is called gamma-ray glows, also known as Thunderstorm Ground Enhancements (TGE) when especially detected at the ground level (Chilingarian et al., 2014). Gamma-ray glows are one of a series of the thundercloud-related energetic events together with Terrestrial Gamma-ray Flashes (TGFs) associated with lightning discharges. TGFs were first reported by Fishman et al. (1994) as gamma-ray burst events with energy ranging up to tens of MeV and a microsecond timescale. The TGFs have been detected both in space and in-ground observations (Briggs et al., 2010; Dwyer et al., 2004; Enoto et al., 2017; Hare et al., 2016; Marisaldi et al., 2010; Smith et al., 2005; Wada et al., 2019). Gamma-ray

glows, on the other hand, are detected from nearby thunderstorms with a minute-long timescale although with lower gamma-ray intensity than TGFs.

Although there is no established theory on the mechanism of neither of TGFs nor gamma-ray glows, a promising concept is the Relativistic Runaway Electron Avalanche (RREA) of exponential multiplication of electrons by electric field (Gurevich et al., 1992) which requires fields strengths stronger than the RREA threshold $E_{th} = 0.284$ MV/m at 1 atm (Babich et al., 2004; Colman et al., 2010; Dwyer, 2003). Under the RREA condition where electrons gain energy from electric fields in the thundercloud environment, the enhancement of gamma-ray flux occurs through the bremsstrahlung interaction of multiplied electrons with the atmospheric particles. Electric fields much stronger than E_{th} may result in a feedback mechanism, in which the electron avalanche becomes self-sustained (Dwyer et al., 2012).

Electric field strengths below the RREA threshold E_{th} do not promote avalanche cascade but provide energy gain with the moving electrons allowing them to move farther away (Diniz et al., 2022) and to increase the gamma-ray production. Chilingarian et al. (2012) proposed the so-called Modification Of Spectra (MOS) mechanism by which such sub-avalanche electric fields ($E < E_{th}$) could generate gamma-ray glows. At this mechanism, an enhancement in a few percentages of gamma-ray production is expected relative to the constant background cosmic-ray air shower. Chilingarian et al. (2012, 2014) also showed that most of the measured gamma-ray glows at Mt. Aragats are related to the MOS mechanism in the sub-avalanche electric fields. On the other hand, strong electric fields of thunderclouds may generate lightning strikes, which would terminate the gamma-ray glows by neutralizing the charged regions and reduce the electric fields. Thus, it is easier to sustain weak electric fields below E_{th} for long time scales (Nicoll, 2012). As shown by these previous studies, the measured spectra of gamma-ray glows are influenced by several ambient atmospheric factors of thunderstorms; the electric field strength (E_S) in the electron acceleration site, the vertical size of this electric field region (H_E), and the vertical size of attenuation region size (H_a). The attenuation region is the area between the bottom of thundercloud electric fields and the ground at which detectors are placed. At the attenuation region, the electron and photon fluxes supposedly most attenuate as there is no applied electric field.

The widely accepted model of thunderstorms assumes a tripolar charge structure with a main positive charge layer at the cloud top, a main negative charge layer in the middle, and a lower positive charge pocket at the bottom (Takahashi, 1978; Williams, 1989). These positions vary according to ambient temperatures. Winter thunderclouds along the sea of Japan are known by the following parameters and ambient conditions; the cloud base altitude is around 0.2–0.8 km (Takahashi, 1978) (i.e., $H_a = 0.2$–0.8 km), the cloud top is in the 5–6 km range indicating compact electric field regions compared with summer thunderstorms with top at ∼14–15 km and base altitude ∼3 km (Wada, Enoto, et al., 2021).

Thanks to the low altitude of winter thunderclouds in Japan, the acceleration region of electrons becomes close to observation sites on the ground (Wada, Enoto, et al., 2021; Wada, Matsumoto, et al., 2021). Thus, winter thunderclouds in Japan are a prone environment to detect gamma-ray glows, which have been explored by the Gamma-Ray Observation of Winter THunderclouds (GROWTH) collaboration. Nevertheless, the ambient parameters of E_S, H_E, and H_a are still highly uncertain as keys to understand and determine the generation mechanism. Thus, the present study exploits the possible environmental parameters through Monte Carlo simulations compared with the observed gamma-ray glow characteristics reported in the catalog of Wada, Matsumoto, et al. (2021). This work is the second paper of a series of studies, starting with (Diniz et al., 2022), which calculated how the electric field strength E_S below RREA threshold E_{th} extends the electron spatial range, in order to develop a general theoretical framework of the gamma-ray glows.

At our computer simulations, we examine how combinations of the three ambient factors (E_S, H_E, H_a) generate gamma-ray spectra and to search for the configuration to reproduce the spectra measured by the GROWTH collaboration providing reference of ambient parameters capable of generating the average observation. The geometry of the simulations is illustrated in Figure 1.

Wada, Matsumoto, et al. (2021) reported spectral fittings of 28 gamma-ray glows with an average form fitted by a cutoff power-law model of,

$$F(\varepsilon) = F_0 \left(\frac{\varepsilon}{1\text{MeV}} \right)^{-\Gamma} \exp\left(-\frac{\varepsilon}{\varepsilon_{\text{cut}}} \right), \quad (1)$$

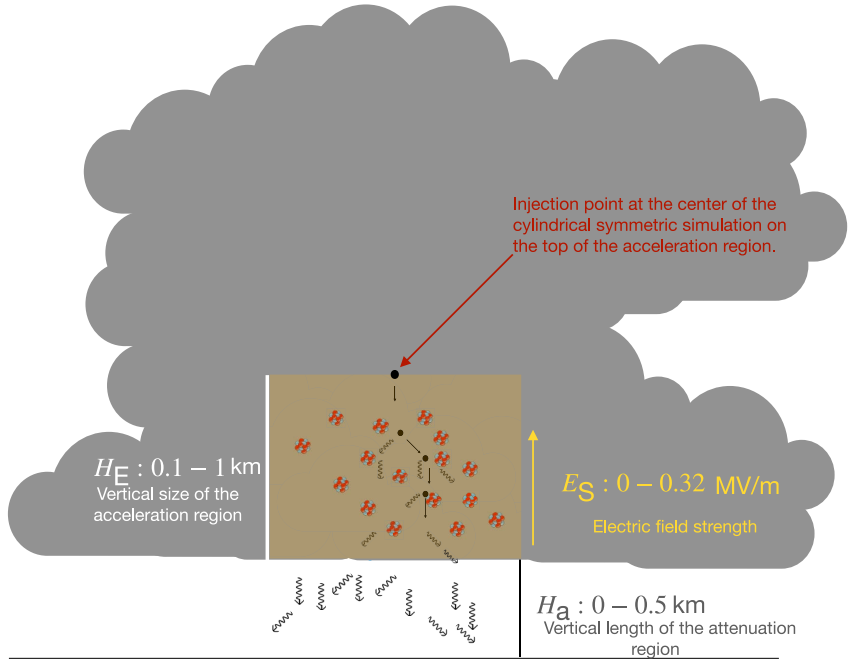

Figure 1. Schematic illustration of the simulated geometry. H_E and E_S are the vertical length and strength of the electric field in the acceleration region. H_a is the attenuation vertical length between the bottom of the electric field and the ground. Here, electrons are represented by black points, while photons are the wiggle lines with arrows. The black horizontal line indicates the level of detectors on the ground.

where ε is the photon energy and $F(\varepsilon)$ is the photon flux in an unit of photons $\mathrm{MeV}^{-1}\ \mathrm{s}^{-1}\ \mathrm{cm}^{-2}$. The reported normalization constant is $F_0 = 0.662 \pm 3.010$ for the energy range of 0.2–20 MeV range. The power-law photon index is $\Gamma = 0.5 \pm 0.28$ and the exponential cutoff energy is $\varepsilon_{\mathrm{cut}} = 4.41 \pm 0.41$ MeV, here the photon flux parameter are the average value from (Wada, Matsumoto, et al., 2021) with the errors being the standard deviation. The average spectrum is shown in Figure 2. It is important to note that the fitting was performed in the 0.6–20 MeV energy range avoiding the annihilation peak at 0.511 MeV but the extrapolated flux is tabulated in the 0.2–20 MeV range.

Gamma-ray fluxes of the 28 gamma-ray glow events (Wada, Matsumoto, et al., 2021) are measured between 1.5×10^{-6} to 8.4×10^{-5} erg $\mathrm{cm}^{-2}\ \mathrm{s}^{-1}$ with a geometric mean of 8.4×10^{-6} erg $\mathrm{cm}^{-2}\ \mathrm{s}^{-1}$ in the 0.2–20 MeV. This information can be used to calculate the model normalization constant, F_0, providing information of the gamma-ray energy flux F_ε (erg $\mathrm{cm}^{-2}\ \mathrm{s}^{-1}$) flux Equations 2–3. Thus, F_ε presented in Wada, Matsumoto, et al. (2021) is used to produce the photon spectra in units of (photons $\mathrm{MeV}^{-1}\ \mathrm{s}^{-1}\ \mathrm{cm}^{-2}$) with F_0,

$$F_\varepsilon = \int_{0.2}^{20} F_0 \varepsilon^{1-\Gamma} e^{\frac{-\varepsilon}{\varepsilon_{\mathrm{cut}}}} d\varepsilon, \tag{2}$$

$$F_0 = \frac{F_\varepsilon}{\int_{0.2}^{20} \varepsilon^{1-\Gamma} e^{\frac{-\varepsilon}{\varepsilon_{\mathrm{cut}}}} d\varepsilon}. \tag{3}$$

In order to directly compare the observations with the simulated results, it is convenient to normalize the spectra by the integrated flux, F_i (photons $\mathrm{s}^{-1}\ \mathrm{cm}^{-2}$),

$$F_i = \int_{0.2}^{20} F(\varepsilon) d\varepsilon, \tag{4}$$

this way, all the spectra presented,$f(\varepsilon)$ in Equation 5, from now on are in standard unit of MeV^{-1} allowing the parallel between the observations and the simulated ambient conditions,

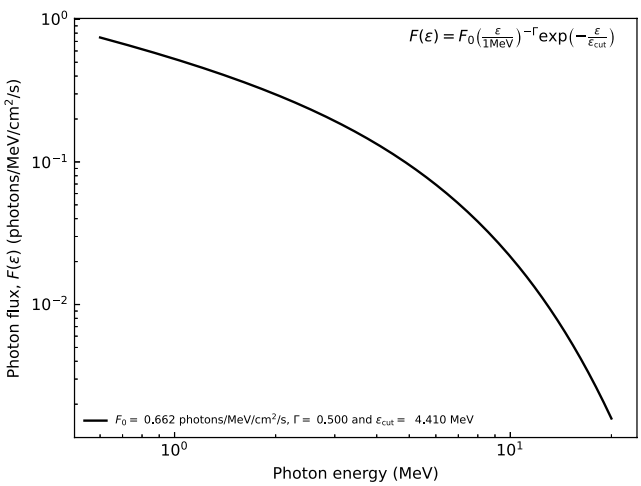

Figure 2. Average gamma-ray glow spectrum observed by Wada, Matsumoto, et al. (2021), the equation in the plot is the used cutoff power-law model.

$$f(\varepsilon) = \frac{F(\varepsilon)}{F_i} = \frac{F_0}{F_i}\left(\frac{\varepsilon}{1\text{MeV}}\right)^{-\Gamma}\exp\left(-\frac{\varepsilon}{\varepsilon_{cut}}\right) = f_0\left(\frac{\varepsilon}{1\text{MeV}}\right)^{-\Gamma}\exp\left(-\frac{\varepsilon}{\varepsilon_{cut}}\right). \quad (5)$$

2. Simulation Setup and Analysis Method

Our simulations were built with GEometry ANd Tracking 4 (GEANT4) version 10.4.3 with the standard "FTFP_BERT_EMZ" physics list including all the necessary processes such as Møller scattering (Agostinelli et al., 2003; Allison et al., 2006, 2016). The simulation geometry is a cylinder with a 20 km radius and 20 km height filled with Standard Temperature and Pressure (STP) air. We used the standard air composition of 78.085% nitrogen, 20.950% oxygen, and 0.965% argon and homogeneous number density of 2.688×10^{25} 1/m^3, equivalent to 1.293 kg/m^3. The geometry includes a cylindrical electric field region with a 15 km radius and its vertical length H_E in the 100–1,000 m range in a simulation step of 100 m for each. We assumed the electric field strength E_S from 0.10 to 0.32 MV/m in a step of 0.01 MV/m including the null electric field ($E_S = 0$) case to be considered a background to be subtracted, thus all simulated spectra produced with $E_S \neq 0$ were subtracted by the spectrum produced with $E_S = 0$ detected at the same level. The simulation geometry is thought with tens of kilometer length scale to avoid boundary issues in the particle recording. The injection point is in the top center of the electric field region, as illustrated in Figure 1, and the detection point is always determined by $H_E + H_a$ vertically away from the injection point which justifies the STP usage since we are evaluating a geometry always below 2 km high. The low-energy threshold of simulations is set to be 0.1 MeV for computation time efficiency. We employed the primary electron spectrum following the EXcel-based Program for calculating Atmospheric Cosmic-ray Spectrum (EXPACS) simulation (Sato, 2015, 2016) in the 1–300 MeV band at 1 km altitude for reference using the coordinates 36°N and 136.5°E from Wada, Matsumoto, et al. (2021) observation site, the simulation design mimics the Japanese winter condition with low-altitude thunderclouds. Since the normalized EXPACS spectra shape does not change substantially in the altitudes of our interest, we use the same input electron shape throughout our simulations even when changing H_a and H_E. The initial energy band of 1–300 MeV is justified by the fact that electron flux sharply decays at higher energies as the cosmic-ray electron flux at this energy band is $\sim 4.47 \times 10^{-3}$ particles s^{-1} cm^{-2} while the flux for electrons with kinetic energy above 1–8.97×10^5 MeV (the EXPACS upper limit) is $\sim 4.66 \times 10^{-3}$ particles s^{-1} cm^{-2}.

We employed two subsequent and independent simulations: (1) Electron and photon spectra are calculated when they exit the electric field region, that is, they are detected at the bottom of the acceleration site. They are recorded to provide the gamma-ray spectra before the attenuation region. As and indicator of the gamma-ray spectral shape we define the spectral hardness η of this data set from the step, assuming a different vertical distance of H_E from the injection point. The hardness η is defined as the following Equation 6,

$$\eta = \frac{\int_{10\ \text{MeV}}^{20\ \text{MeV}} f(\varepsilon)d\varepsilon}{\int_{1\ \text{MeV}}^{10\ \text{MeV}} f(\varepsilon)d\varepsilon}, \quad (6)$$

where $f(\varepsilon)$ is the gamma flux as a function of energy. Thus, the simulated spectral hardness is obtained by counting the photons in the energy ranges of 1–10 MeV and 10–20 MeV. We obtain the hardness of the observed spectra as a function of the fitting parameters by implementing Equation 1 to Equation 6;

$$\eta(\Gamma, \varepsilon_{cut}) = \frac{\int_{10\ \text{MeV}}^{20\ \text{MeV}} \varepsilon^{-\Gamma} e^{\frac{-\varepsilon}{\varepsilon_{cut}}} d\varepsilon}{\int_{1\ \text{MeV}}^{10\ \text{MeV}} \varepsilon^{-\Gamma} e^{\frac{-\varepsilon}{\varepsilon_{cut}}} d\varepsilon}. \quad (7)$$

We use the hardness ratio η to filter out the geometry pairs (E_S, H_E) that can not produce the observed gamma-ray glow spectrum after exiting the acceleration region.

The second simulation set (2) repeats the geometry of set (1) but only for the pairs (E_S, H_E) that are able to produce the observed gamma-ray glow spectrum with the inclusion of an attenuation region with vertical size $H_a = 0.1$–0.5 km in steps of 0.1 km for each simulation to better replicate the observed gamma-ray glow spectra. In particular, after leaving the electric field region, the electrons will attenuate without any energy gain which will reduce also photon yield in comparison to the production within electrified regions. Thus, once the electrons and

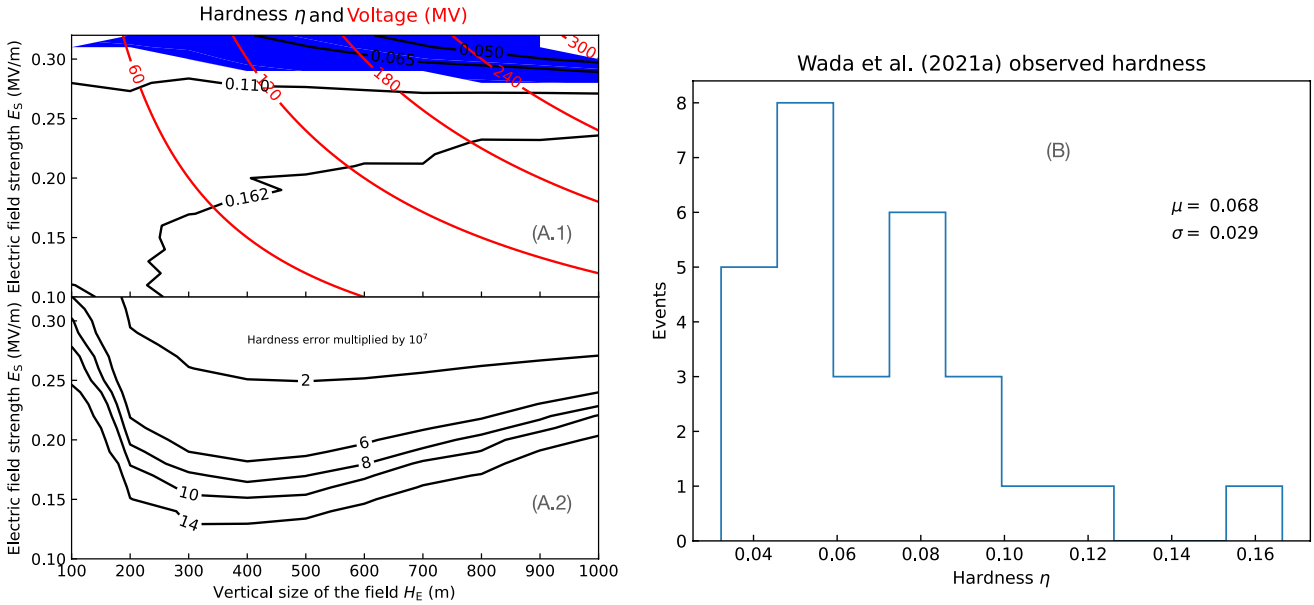

Figure 3. (a) Simulated spectral hardness η at the bottom of the acceleration region (black curves on a.1) as function of E_S and H_E. Voltage difference in the acceleration region as a product $E_S \times H_E$ is represented by the red lines. The blue region indicates the one σ region of observed hardness ($\mu \pm \sigma$, where μ is the mean of panel B and σ the standard deviation) reported in (Wada, Matsumoto, et al., 2021). The bottom panel (a.2) displays errors of the hardness η evaluated via Poisson statistics. The values in contours are shown after multiplied by 10^7. The panel (B) is histogram of the hardness η of the 28 gamma-ray glows used by Wada, Matsumoto, et al. (2021).

photons enter the attenuation region, the lower energy end of the spectra will vanish faster than the high energy portion due to the difference in the spatial range as a function of energy, as shown in Figure 4. This effect implies that the attenuation region only increases the spectra hardness η.

The computational cost for our simulations increases by the number of initial electrons or the applied electric field strength. Thus, for a precision compromise, we use 10^5 initial electrons and limit the electric field up to 0.32 MV m^{-1} slightly higher than E_{th}. Chilingarian et al. (2014) and Cramer et al. (2017) use a similar approach since most gamma-ray glows or TGEs are not expected to require much stronger electric fields than this value.

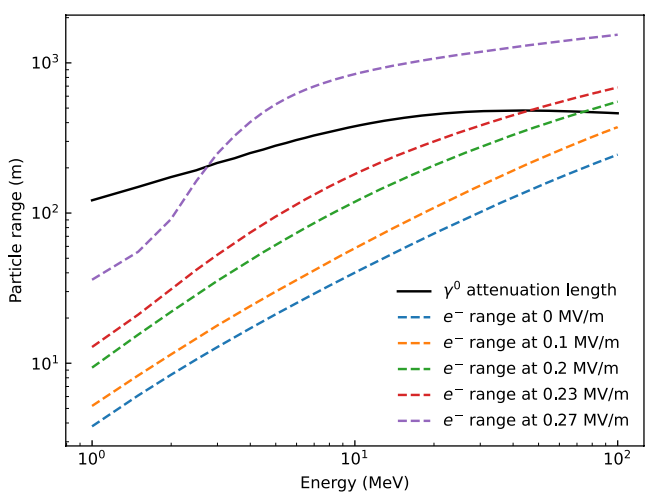

Figure 4. Electron ranges (dashed lines) as function of electron kinetic energy at different electric field strength (legend in the figure) below the RREA threshold (Diniz et al., 2022). The photon attenuation length is also shown (solid black line) from the NIST database (https://physics.nist.gov/PhysRefData/Xcom/html/xcom1.html).

We selected our parameter range to resemble the geometric conditions of the winter thundercloud in Japan, that is, the thundercloud is not only compact but also has a low base altitude (Wada, Enoto, et al., 2021). Thus, larger values of H_E, H_a, and E_S than our range might be unlikely configurations for thunderstorms of our targets. At the present simulation setup, we record the modified gamma-ray and electron spectra at a vertical distance of $H_E + H_a$ away from the injection point source, as illustrated in Figure 1, in order to find possible configurations that generate the observed functional form.

3. Ambient Condition Effects on Simulated Parameters

At first, we searched for a pair of electric field strength (E_S) and electric field vertical length (H_E) which produce a similar spectral shape as the observed one using the hardness η. Figure 3a shows a contour map of hardness values at different electric field magnitudes and lengths in comparison to the observed data (Wada, Matsumoto, et al., 2021). Different combinations of the pair (E_S, H_E) produce gamma-ray spectra with the same hardness as Cramer et al. (2017) also already noted.

The spectra analyzed in the first simulation set with hardness higher than the observed level ($\eta \sim 0.039$–0.097) are unable to produce the reported gamma-ray glow spectrum. Thus, we filter the possible pairs (E_S, H_E) to only those with softer hardness values below the maximum observed level, that is,

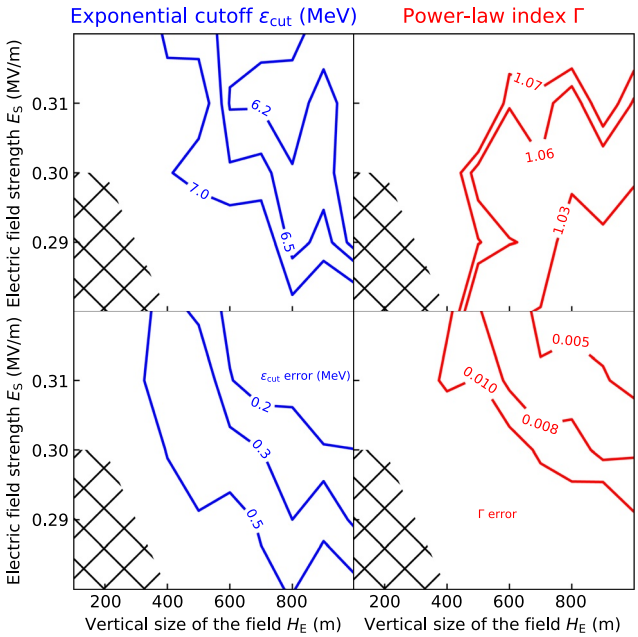

Figure 5. Contour maps of the cutoff power-law model parameters (Equation 1). The energy cutoff ε_{cut} (left) and the photon index Γ (right) are in the first row, while the associated errors are shown in the second row. The errors are the square root of the covariance matrix diagonal terms. The hatched area is the region where the hardness η is higher than the observed hardness ($\eta > \mu + \sigma$), as shown in Figure 3, indicating configurations that are not able to reproduce the observations.

$\eta \leq 0.097$, being μ and σ the average observed hardness and the associated standard deviation indicated at Figure 3b, respectively. Using this filter, we limited our grid to $E_S = 0.28$–0.32 MV/m and $H_E = 100$–$1{,}000$ m.

We use the filtered data to evaluate the spectral parameters in Figure 5. This figure shows contour maps of the energy cutoff ε_{cut} and photon index Γ as function of electric field strength E_S and vertical length H_E. Figure 5 shows that ε_{cut} from Equation 1 declines from ~10 to ~5 MeV as the pair (E_S, H_E) increase, since the electric field levels around E_{th} increase the low-energy particles population relatively further than the high-energy ones. This indicates that the average observed gamma-ray glow requires an electric field strength close to the RREA threshold E_{th} or even higher than the upper end of our data grid as Figure 3 also shows. The energy cutoff ε_{cut} agrees with the previously studied RREA formulation (Coleman & Dwyer, 2006; Dwyer, 2003), in which the average RREA energy cutoff should be close to 7 MeV. At electric fields close to the RREA threshold, the value becomes lower than 7 MeV.

On the other hand, the photon index Γ behavior is more complex. It does not vary substantially with the pair (E_S, H_E) but there is a slightly tendency for Γ to increase with E_S and decrease with H_E. The amplification in the acceleration region with electric field strength E_S happens with an increase of the low-energy electron and photon populations production since the low-energy electrons are kept above the low-energy simulation threshold and keep emitting low-energy photons. This effect is a reflex of the low-energy biasing of both production processes, bremsstrahlung for photons and Møller scattering for electrons (Sarria et al., 2018). While an increasing H_E elongates the electron path it still is a distance in which photons attenuate, thus there is still a significant energy loss as the data grid is close to the RREA threshold in longs H_E.

At the bottom of the acceleration region, the photon indices are greater (Γ ~ 1.00–1.09) than the observed interval (Γ ~ 0.22–0.78) reported from the GROWTH collaboration (Wada, Matsumoto, et al., 2021). Figure 6 shows background-subtracted simulated spectra of four pairs (E_S, H_E) further modified by an increasing H_a. The attenuation region with a vertical length (H_a) without an electric field reduces the indices, that is the spectra hardness η increases, because it attenuates low-energy photons and electrons that would source other low-energy photons. Figure 6 indicates how increasing H_a approximates the original spectra toward the average observed one.

We simulated 194 data points of (E_S, H_E, H_a). Only two triads among all simulated geometries can produce acceptable spectra to explain all fitting parameters (f_0, Γ, ε_{cut}) within one sigma from the observation values: (E_S, H_E, H_a) = (0.30 MV/m, 900 m, 300 m) and (0.31 MV/m, 1,000 m, 400 m). Figure 7 shows the hardness η, photon index Γ, energy cutoff ε_{cut}, and normalization f_0 as function of H_a for the two (E_S, H_E) pairs, (0.30 MV/m, 900 m) and (0.31 MV/m, 1,000 m). Although the two triads, (0.30 MV/m, 900 m, 300 m) and (0.31 MV/m, 1,000 m, 400 m), have all the fitting parameters inside the observational ranges, the latter has the hardness closer to the observed average value replicating the observed gamma-ray glow spectrum better than the former triad.

Finally, Figure 8 shows the comparison between the spectrum produced by both best triads, (0.31 MV/m, 1,000 m, 400 m) and (0.30 MV/m, 900 m, 300 m), and the observed gamma-ray glow spectrum. While the simulated spectra in Figure 8 has all the analyzed quantities (hardness η, normalization f_0, photon index Γ, energy cutoff ε_{cut}) within the observations ranges, the ratio between the simulated fitted and average observed curves ranges from 0.85 to 1.15 (Figure 8 bottom). Considering the RREA avalanche length calculated by Dwyer (2003), the best fitting triads have ~4.65 (considering the configuration, 0.31 MV/m, 1,000 m, 400 m) and 2.96 (considering the configuration, 0.30 MV/m, 900 m, 300 m) avalanche lengths to develop, which is not sufficient to reach steady state (Coleman & Dwyer, 2006; Dwyer, 2003), thus we must consider that RREAs related to the observed gamma-ray glow should be under-developed. Our results indicate that the cosmic-ray interaction with the thundercloud environment is sufficient to generate the gamma-ray glow without another external injection source. Our results are bounded by the discrete data grid of simulation parameters. In reality, the triad parameters (E_S, H_E, H_a) may vary continuously and, hence other triads are possible.

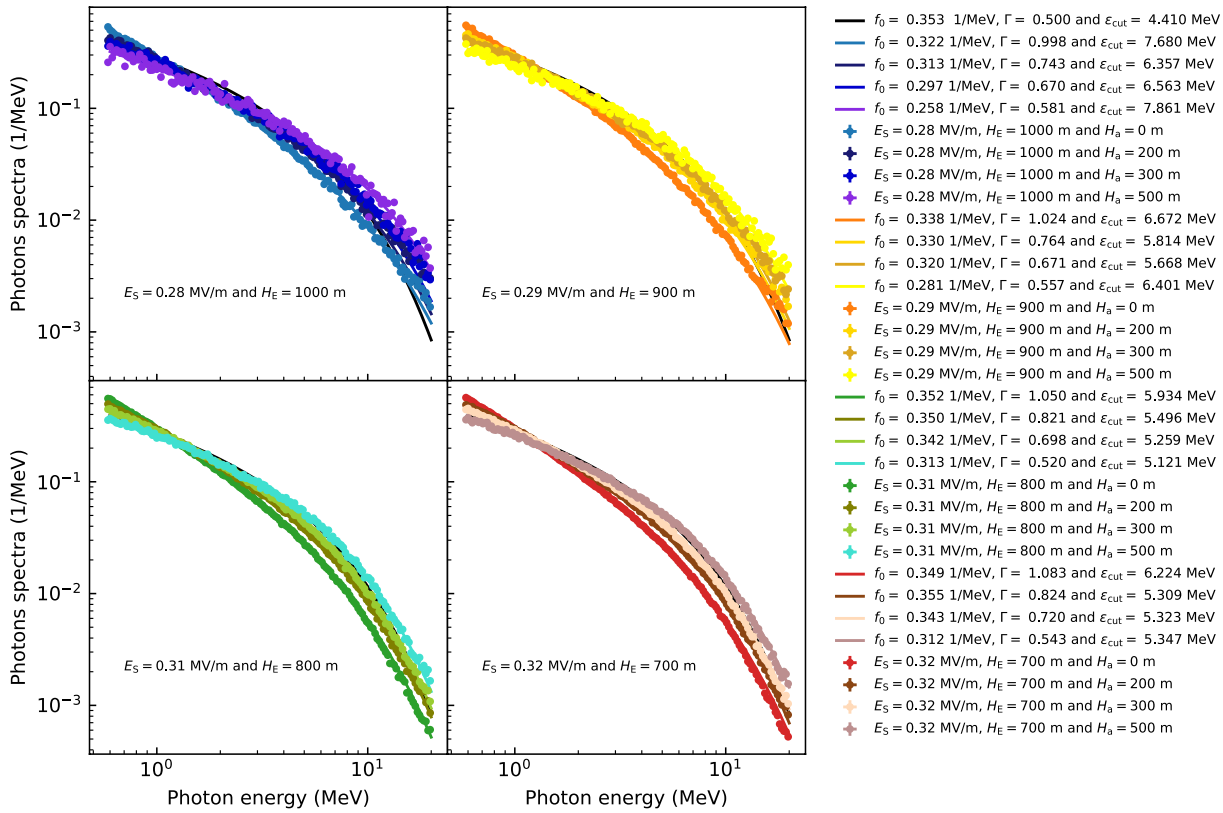

Figure 6. Examples of spectra produced by four pairs of (E_S, H_E). Simulation parameters are indicated in the subplots with the legends, compared with the average observed spectrum (black curve same as Figure 2). At each subplot, spectra are modified by the increasing attenuation region of the vertical length (H_a). The legend indicates each curve geometry and fitting parameters.

It is important to emphasize that the results are calculated regarding the STP air density in this paper. Our results are scalable to atmospheric depth for adaptation to any density taking in consideration the variation of E_{th} with the density (Dwyer, 2003) which may also alter the E_S levels. The atmospheric density inhomogeneity may generate isolated RREA regions near the source altitude although the small density variation for the considered heights. This investigation is reserved for future works following the series of studies started with Diniz et al. (2022).

4. Comparison Between Different Glow Mechanisms

The two main proposed gamma-ray glow mechanisms are MOS and RREA (Chilingarian et al., 2014; Cramer et al., 2017), but distinguishing one from another is rather challenging. A fundamental difference is the electric field strength E_S below or above the RREA threshold of $E_{th} = 0.284$ MV m^{-1}. The strong electric field ($E_S \geq E_{th}$) will induce an avalanche behavior in the electron population with exponential growth and, hence, there will still produce bremsstrahlung emissions as long as there is sufficiently high E_S. On the other hand, weaker electric fields ($E_S \leq E_{th}$) simply extend the finite electrons spatial range through a friction reduction (Diniz et al., 2022; Lehtinen & Østgaard, 2018), meaning that both electron and photon generation will be finite even inside the electrified region due to the lack of avalanches.

In particular, gamma-ray glow generated by weaker fields tend to still hold a power-law spectral form, while RREA induces the cutoff power-law shape (Chilingarian et al., 2014; Cramer et al., 2017), as our results indicate that decreasing electric field strength E_S increase energy cutoff ε_{cut} (Figure 5). Ideally, a sufficiently low E_S would lead to an infinite ε_{cut} which would modify the cutoff power-law model from Equation 1 to a convolution of power-laws. In the first approximation, ε_{cut} can be interpreted as a consequence of the intersection between the applied electric field and the friction curve, particularly, once the spatial scattering is included (Lehtinen & Østgaard, 2018).

Finally, through several gamma-ray glow or TGE measurements (Chilingarian, 2013; Chilingarian et al., 2011, 2014, 2017), a higher photon flux is expected in RREA situations in comparison to MOS yield.

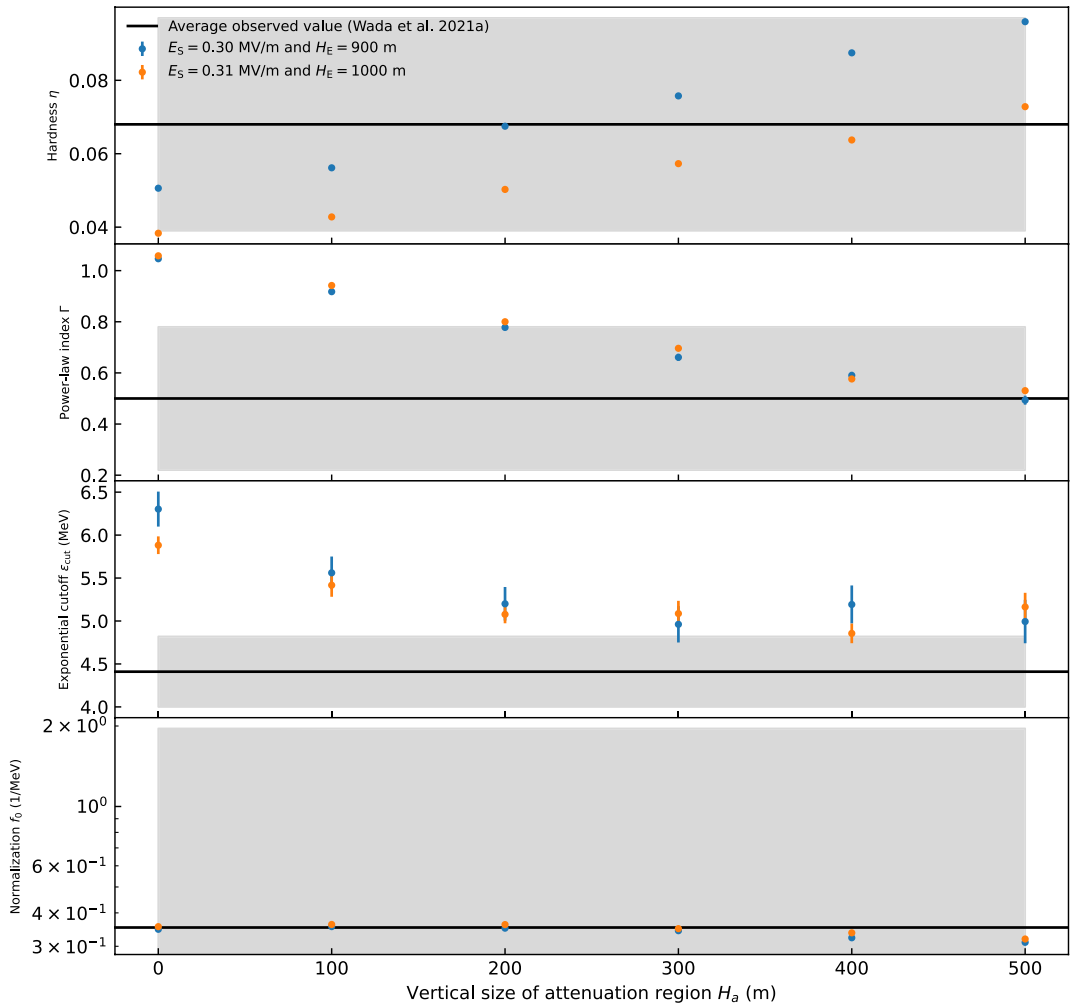

Figure 7. Hardness η (first panel), photon index Γ (second panel), cutoff energy ε_{cut} (third panel), and photon flux f_0 (fourth panel) as a function of the attenuation vertical length (H_a) assuming the best two parameter pairs (E_S, H_E) of (0.30 MV/m, 900 m) and (0.31 MV/m, 1,000 m), shown as blue and orange points, respectively. The errors related with η, Γ and f_0 are too small and thus are not visible in these plots. The solid black lines are the observed average parameters, while the light gray areas represent one sigma regions for each observed parameter.

The current paper evaluations indicate that the average gamma-ray glow from the GROWTH catalog (Wada, Matsumoto, et al., 2021) requires an RREA mechanism as the spectra follow a cutoff power-law model and a photon flux with orders of magnitude above the ones retrieved from ambient conditions with $E_S \leq E_{th}$. Differently from observation at Mt. Aragats (Chilingarian et al., 2012, 2014, 2017), GROWTH measurements in Japan are on-ground measurements at almost the sea level, which introduces $H_a > 0$ reducing the power-law index and modifying the low-energy spectral end.

5. Conclusion

We have explored the ambient geometry and conditions through GEANT4 simulations testing the electric field strength and its size (E_S, H_E) phase space to reproduce the spectral form of the gamma-ray glow observations performed by the GROWTH collaboration (Wada, Matsumoto, et al., 2021). It is shown that not all (E_S, H_E) are capable of producing the cutoff power-law form (Equation 1). But, close to the RREA threshold E_{th}, the exponential cutoff energy is a function of (E_S, H_E) with a negative gradient to them. The attenuation region, with vertical length H_a, is used for adjustment of the spectral slope and we have demonstrated that it decreases the spectral power-law index, approximating the simulated spectra to the observed cutoff power-law model, Equation 1. The existence of $H_a > 0$ shows that electric fields close to the detection site at the sea level must be weak to allow such

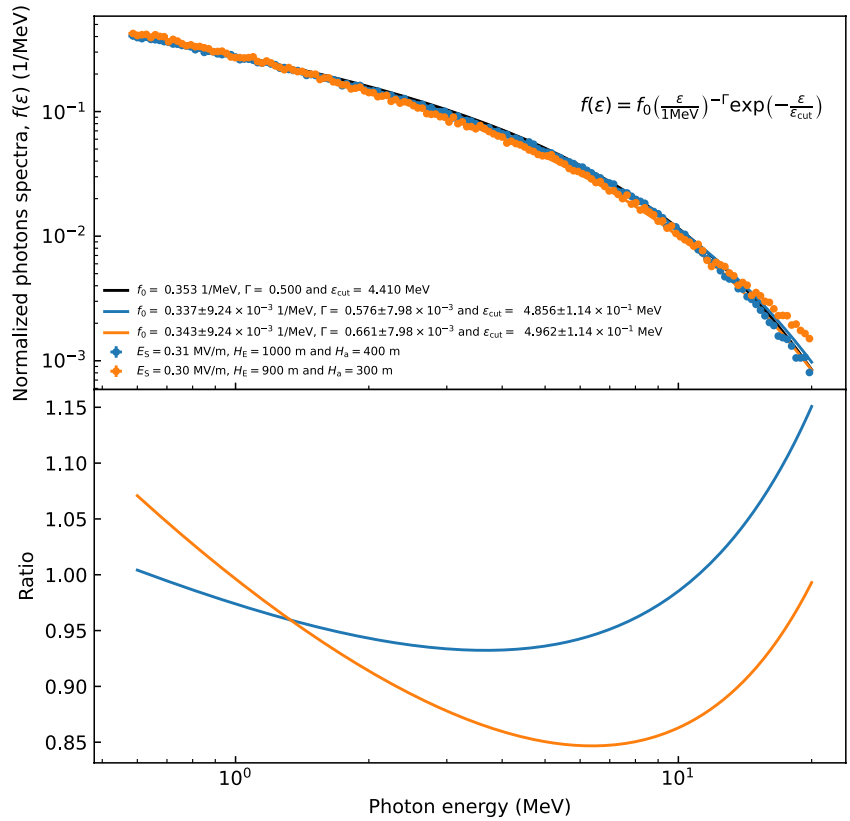

Figure 8. In the upper panel, background-subtracted simulated spectrum of gamma-ray glows (blue points) closest to the average observed spectral shape. The simulated data are normalized by the integrated flux and fitted with exponential cutoff power-law model (blue curve same as Figure 2). In the bottom panel, the ratio between the simulated fit and the average observed spectrum is present in the lower panel.

power-law index attenuation as it does not vary substantially in the presence of electric fields strengths close to E_{th} being $\Gamma \sim 1.05$.

Several ambient combinations of (E_S, H_E, H_a) are capable of generating the observed spectral form with some indications; E_S must be close to the RREA threshold E_{th}, H_E must be comparable to 1 km to allow electron multiplication but not so large to prevent attenuation of the photons that are generated along the whole path. H_a must be large enough (~400 m) to attenuate the low particles and decrease the power-law index. In particular, two triad sets of (E_S, H_E, H_a) replicates the observed gamma-ray glow within the one sigma, (0.30 MV/m, 900 m, 500 m) and (0.31 MV/m, 1,000 m, 400 m).

Data Availability Statement

The simulations of this work use the GEANT4 version 10.4.3 available at, https://geant4.web.cern.ch. The data regarding the present analysis is at the data set Diniz and Enoto (2023).

Acknowledgments
This work G.S.D. and T.E. are supported by Hakubi Research Project and MEXT/JSPS KAKENHI Grants 19H00683, 22KF0190, and 22H00145; Y.W. is supported by KAKENHI Grants 21H01116 and 22K14453. K.N. is supported by the KAKENHI Grant 21H00166. Y.O. is supported by the KAKENHI Grants 19H01893 and 21H04487. The simulations of this work were done with the RIKEN BIG WATERFALL HOKUSAI computer system.

References

Agostinelli, S., Allison, J., Amako, K., Apostolakis, J., Araujo, H., Arce, P., et al. (2003). GEANT4: A simulation toolkit. *Nuclear Instruments & Methods*, *A506*(3), 250–303. https://doi.org/10.1016/S0168-9002(03)01368-8

Allison, J., Amako, K., Apostolakis, J., Araujo, H., Arce Dubois, P., Asai, M., et al. (2006). Geant4 developments and applications. *IEEE Transactions on Nuclear Science*, *53*(1), 270–278. https://doi.org/10.1109/tns.2006.869826

Allison, J., Amako, K., Apostolakis, J., Arce, P., Asai, M., Aso, T., et al. (2016). Recent developments in Geant4. *Nuclear Instruments and Methods in Physics Research Section A: Accelerators, Spectrometers, Detectors and Associated Equipment*, *835*, 186–225. https://doi.org/10.1016/j.nima.2016.06.125

Babich, L. P., Donskoy, E. N., Il'kaev, R. I., Kutsyk, I. M., & Roussel-Dupre, R. A. (2004). Fundamental parameters of a relativistic runaway electron avalanche in air. *Plasma Physics Reports*, *30*(7), 616–624. https://doi.org/10.1134/1.1778437

Briggs, M. S., Fishman, G. J., Connaughton, V., Bhat, P. N., Paciesas, W. S., Preece, R. D., et al. (2010). First results on terrestrial gamma ray flashes from the fermi gamma-ray burst monitor. *Journal of Geophysical Research*, *115*(A7), A07323. https://doi.org/10.1029/2009JA015242

Chilingarian, A. (2013). Thunderstorm ground enhancements (TGEs) - New high-energy phenomenon originated in the terrestrial atmosphere. *Journal of Physics: Conference Series*, *409*(1), 012019. https://doi.org/10.1088/1742-6596/409/1/012019

Chilingarian, A., Hovsepyan, G., & Hovhannisyan, A. (2011). Particle bursts from thunderclouds: Natural particle accelerators above our heads. *Physical Review D*, *83*(6), 062001. https://doi.org/10.1103/PhysRevD.83.062001

Chilingarian, A., Hovsepyan, G., & Vanyan, L. (2014). On the origin of the particle fluxes from the thunderclouds: Energy spectra analysis. *EPL*, *106*(5), 59001. https://doi.org/10.1209/0295-5075/106/59001

Chilingarian, A., Khanikyants, Y., Mareev, E., Pokhsraryan, D., Rakov, V. A., & Soghomonyan, S. (2017). Types of lightning discharges that abruptly terminate enhanced fluxes of energetic radiation and particles observed at ground level. *Journal of Geophysical Research: Atmospheres*, *122*(14), 7582–7599. https://doi.org/10.1002/2017JD026744

Chilingarian, A., Mailyan, B., & Vanyan, L. (2012). Recovering of the energy spectra of electrons and gamma rays coming from the thunderclouds. *Atmospheric Research*, *114–115*, 1–16. https://doi.org/10.1016/j.atmosres.2012.05.008

Coleman, L. M., & Dwyer, J. R. (2006). Propagation speed of runaway electron avalanches. *Geophysical Research Letters*, *33*(11), L11810. https://doi.org/10.1029/2006GL025863

Colman, J. J., Roussel-Dupré, R. A., & Triplett, L. (2010). Temporally self–similar electron distribution functions in atmospheric breakdown: The thermal runaway regime. *Journal of Geophysical Research*, *115*(A3), A00E16. https://doi.org/10.1029/2009JA014509

Cramer, E. S., Mailyan, B. G., Celestin, S., & Dwyer, J. R. (2017). A simulation study on the electric field spectral dependence of thunderstorm ground enhancements and gamma ray glows. *Journal of Geophysical Research: Atmospheres*, *122*(9), 4763–4772. https://doi.org/10.1002/2016JD026422

Diniz, G., Wada, Y., Ohira, Y., Nakazawa, K., & Enoto, T. (2022). Atmospheric electron spatial range extended by thundercloud electric field below the relativistic runaway electron avalanche threshold. *Journal of Geophysical Research: Atmospheres*, *127*(3), e2021JD035. https://doi.org/10.1029/2021JD035958

Diniz, G. S., & Enoto, T. (2023). Ambient conditions gamma-ray glow compared with growth observations [dataset]. Mendeley. https://doi.org/10.17632/67h7rgjvys.2

Dwyer, J. R. (2003). A fundamental limit on electric fields in air. *Geophysical Research Letters*, *30*(20), 2055. https://doi.org/10.1029/2003GL017781

Dwyer, J. R., Rassoul, H. K., Al-Dayeh, M., Caraway, L., Wright, B., Chrest, A., et al. (2004). A ground level gamma-ray burst observed in association with rocket-triggered lightning. *Geophysical Research Letters*, *31*(5), L05119. https://doi.org/10.1029/2003GL018771

Dwyer, J. R., Smith, D. M., & Cummer, S. A. (2012). High-energy atmospheric physics: Terrestrial gamma-ray flashes and related phenomena. *Space Science Reviews*, *173*(1–4), 133–196. https://doi.org/10.1007/s11214-012-9894-0

Enoto, T., Wada, Y., Furuta, Y., Nakazawa, K., Yuasa, T., Okuda, K., et al. (2017). Photonuclear reactions triggered by lightning discharge. *Nature*, *551*(7681), 481–484. https://doi.org/10.1038/nature24630

Fishman, G. J., Bhat, P. N., Mallozzi, R., Horack, J. M., Koshut, T., Kouveliotou, C., et al. (1994). Discovery of intense gamma-ray flashes of atmospheric origin. *Science*, *264*(5163), 1313–1316. https://doi.org/10.1126/science.264.5163.1313

Gurevich, A., Milikh, G., & Roussel-Dupre, R. (1992). Runaway electron mechanism of air breakdown and preconditioning during a thunderstorm. *Physics Letters A*, *165*(5), 463–468. https://doi.org/10.1016/0375-9601(92)90348-P

Hare, B. M., Uman, M. A., Dwyer, J. R., Jordan, D. M., Biggerstaff, M. I., Caicedo, J. A., et al. (2016). Ground-level observation of a terrestrial gamma ray flash initiated by a triggered lightning. *Journal of Geophysical Research: Atmospheres*, *121*(11), 6511–6533. https://doi.org/10.1002/2015JD024426

Kelley, N. A., Smith, D. M., Dwyer, J. R., Splitt, M., Lazarus, S., Martinez-McKinney, F., et al. (2015). Relativistic electron avalanches as a thunderstorm discharge competing with lightning. *Nature Communications*, *6*(1), 7845. https://doi.org/10.1038/ncomms8845

Kochkin, P., van Deursen, A. P. J., Marisaldi, M., Ursi, A., de Boer, A. I., Bardet, M., et al. (2017). In-flight observation of gamma ray glows by ildas. *Journal of Geophysical Research: Atmospheres*, *122*(23), 12801–12811. https://doi.org/10.1002/2017JD027405

Lehtinen, N. G., & Østgaard, N. (2018). X-ray emissions in a multiscale fluid model of a streamer discharge. *Journal of Geophysical Research: Atmospheres*, *123*(13), 6935–6953. https://doi.org/10.1029/2018JD028646

Marisaldi, M., Fuschino, F., Labanti, C., Galli, M., Longo, F., Del Monte, E., et al. (2010). Detection of terrestrial gamma ray flashes up to 40 MeV by the agile satellite. *Journal of Geophysical Research*, *115*(A3), A00E13. https://doi.org/10.1029/2009JA014502

Nicoll, K. A. (2012). Measurements of atmospheric electricity aloft. *Surveys in Geophysics*, *33*(5), 991–1057. https://doi.org/10.1007/s10712-012-9188-9

Østgaard, N., Christian, H. J., Grove, J. E., Sarria, D., Mezentsev, A., Kochkin, P., et al. (2019). Gamma ray glow observations at 20-km altitude. *Journal of Geophysical Research: Atmospheres*, *124*(13), 7236–7254. https://doi.org/10.1029/2019JD030312

Sarria, D., Rutjes, C., Diniz, G., Luque, A., Ihaddadene, K. M. A., Dwyer, J. R., et al. (2018). Evaluation of Monte Carlo tools for high-energy atmospheric physics ii: Relativistic runaway electron avalanches. *Geoscientific Model Development*, *11*(11), 4515–4535. https://doi.org/10.5194/gmd-11-4515-2018

Sato, T. (2015). Analytical model for estimating terrestrial cosmic ray fluxes nearly anytime and anywhere in the world: Extension of PARMA/EXPACS. *PLoS One*, *10*(12), 1–33. https://doi.org/10.1371/journal.pone.0144679

Sato, T. (2016). Analytical model for estimating the zenith angle dependence of terrestrial cosmic ray fluxes. *PLoS One*, *11*(8), 1–22. https://doi.org/10.1371/journal.pone.0160390

Smith, D. M., Lopez, L. I., Lin, R. P., & Barrington-Leigh, C. P. (2005). Terrestrial gamma-ray flashes observed up to 20 MeV. *Science*, *307*(5712), 1085–1088. https://doi.org/10.1126/science.1107466

Takahashi, T. (1978). Riming electrification as a charge generation mechanism in thunderstorms. *Journal of the Atmospheric Sciences*, *35*(8), 1536–1548. https://doi.org/10.1175/1520-0469(1978)035<1536:REAACG>2.0.CO;2

Torii, T., Takeishi, M., & Hosono, T. (2002). Observation of gamma-ray dose increase associated with winter thunderstorm and lightning activity. *Journal of Geophysical Research*, *107*(D17), ACL2-1–ACL2-13. https://doi.org/10.1029/2001JD000938

Tsuchiya, H., Enoto, T., Yamada, S., Yuasa, T., Kawaharada, M., Kitaguchi, T., et al. (2007). Detection of high-energy gamma rays from winter thunderclouds. *Physical Review Letters*, *99*(16), 165002. https://doi.org/10.1103/PhysRevLett.99.165002

Tsuchiya, H., Hibino, K., Kawata, K., Hotta, N., Tateyama, N., Ohnishi, M., et al. (2012). Observation of thundercloud-related gamma rays and neutrons in Tibet. *Physical Review D*, *85*(9), 092006. https://doi.org/10.1103/PhysRevD.85.092006

Wada, Y., Bowers, G. S., Enoto, T., Kamogawa, M., Nakamura, Y., Morimoto, T., et al. (2018). Termination of electron acceleration in thundercloud by intracloud/intercloud discharge. *Geophysical Research Letters*, *45*(11), 5700–5707. https://doi.org/10.1029/2018GL077784

Wada, Y., Enoto, T., Kubo, M., Nakazawa, K., Shinoda, T., Yonetoku, D., et al. (2021). Meteorological aspects of gamma-ray glows in winter thunderstorms. *Geophysical Research Letters*, *48*(7), e2020GL091. https://doi.org/10.1029/2020GL091910

Wada, Y., Enoto, T., Nakamura, Y., Furuta, Y., Yuasa, T., Nakazawa, K., et al. (2019). Gamma-ray glow preceding downward terrestrial gamma-ray flash. *Communications Physics*, *2*(1), 67. https://doi.org/10.1038/s42005-019-0168-y

Wada, Y., Matsumoto, T., Enoto, T., Nakazawa, K., Yuasa, T., Furuta, Y., et al. (2021). Catalog of gamma-ray glows during four winter seasons in Japan. *Physical Review Research*, *3*(4), 043117. https://doi.org/10.1103/PhysRevResearch.3.043117

Williams, E. R. (1989). The tripole structure of thunderstorms. *Journal of Geophysical Research*, *94*(D11), 13151–13167. https://doi.org/10.1029/JD094iD11p13151